Formation of Multiple Complexes between Actinomycin D and a DNA Hairpin: Structural Characterization by Multinuclear NMR†

David R. Brown,‡ Michael Kurz,§ David R. Kearns,* and Victor L. Hsu*,‖

Department of Chemistry, 0342, University of California, San Diego, 9500 Gilman Drive, La Jolla, California 92093-0342

Received August 24, 1993⊛

ABSTRACT: The solution conformations of a DNA oligomer and its complexes with the anticancer drug actinomycin D (ActD) were characterized using homo- and heteronuclear NMR techniques. Previous high-resolution NMR investigations of ActD–DNA complexes employed symmetric double-stranded DNA oligomers, yielding two identical symmetry-related complexes. In order to understand the important effects that neighboring base pairs and/or unusual nucleic acid structures may have on ActD binding specificity and orientation, we chose to study the oligonucleotide d(TCGCGTTTTCGCGA), which adopts a hairpin structure in solution. NOE cross-peak intensities were used to generate distance constraints for molecular dynamics simulations and structure determinations of the free oligonucleotide and for both complexes. A total of 86 intermolecular NOEs were identified for each complex, 27 of which involve exchangeable protons. These intermolecular NOEs along with changes in the phosphorus chemical shifts were used to determine the drug binding site on the DNA. As expected, ActD intercalated exclusively at the single d(GC) step in the DNA hairpin. Interestingly, although the two complexes, which differ by the orientation with which the asymmetric drug chromophore intercalates the DNA, were not formed in equal concentrations, their conformations are very similar. The RMS difference of the DNA hairpin in the two complexes is only 1.10 Å. The structures of the minor groove binding pentapeptide rings are not affected by any of the changes in the normal double-helical structure imposed by the hairpin loop. The total pairwise RMS difference over all atoms for the four peptides (two per complex) in the calculated structures is 0.72 Å. Conversely, the structure of the hairpin loop is not appreciably changed upon binding—the RMS difference between the free DNA loop region and the loop region in the two complexes is 1.68 Å and only 0.43 Å between the two complexes. Our data also support a possible conformation of the $d(T)_4$ loop that does not possess a thymine–thymine "wobble" base pair.

Actinomycin D (ActD)[1] is a very potent antitumor drug (Figure 1) that has been used clinically for treating certain types of cancer. Its molecular mechanism of action has been attributed to its ability to bind to double-stranded DNA, resulting in the inhibition of DNA-directed RNA synthesis (Kirk, 1960; Reich et al., 1961; Goldberg & Rabinowitz, 1962; Mauger, 1980). The mode of binding involves intercalation of the phenoxazone chromophore between base pairs in duplex DNA via the minor groove (Muller & Crothers, 1968; Waring, 1970). The X-ray crystal structure of ActD complexed with deoxyguanosine was solved by Jain and Sobell (1972). The details of this crystal structure were used to suggest a molecular model for the ActD–$d(ATGCAT)_2$ complex, which provided the first indication that the chromophore shows high specificity

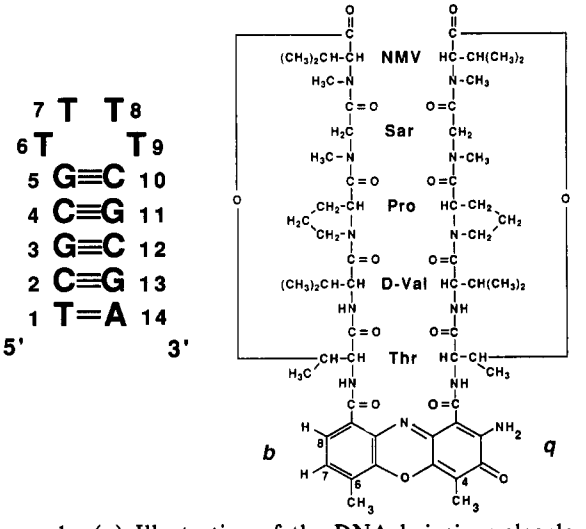

FIGURE 1: (a) Illustration of the DNA hairpin molecule d-(TCGCGTTTTCGCGA); (b) actinomycin D structure. b = benzenoid side of phenoxazone ring; q = quinoid side of phenoxazone ring.

for intercalating d(GC) sites and that the two cyclic pentapeptide lactone moieties bind in the minor groove (Sobell & Jain, 1972; Sobell, 1985). The sequence specificity of ActD for d(GC) sites has also been confirmed by DNAse I footprinting studies (Lane et al., 1983; Fox & Waring, 1984; Rehfuss et al., 1990).

The model proposed for the binding of ActD to DNA is one in which the chromophore intercalates at a d(GC) site, with the complex stabilized by a strong hydrogen bond between an

† Supported by a grant from the American Cancer Society (ACS DHP-240). NMR instrumentation was provided by grants from the NIH (1S01 RR03342) and the NSF (BBS86-12359).

* Authors to whom correspondence should be addressed.

‡ Current address: Office of Academic Enrichment 0074, University of California, San Diego, La Jolla, CA 92093-0074.

§ Current address: Lepetit Research Center, Analytical Department, Via R. Lepetit 34, 21040 Gerenzano (Varese), Italy.

‖ Current address: Department of Biochemistry and Biophysics, Oregon State University, Corvallis, OR 97331.

⊛ Abstract published in *Advance ACS Abstracts,* November 1, 1993.

[1] Abbreviations: 1D, one dimensional; 2D, two dimensional; ActD, actinomycin D; COSY, correlated spectroscopy; DQF-COSY, double-quantum filtered COSY; DNA, deoxyribonucleic acid; HMQC, heteronuclear multiple-quantum coherence spectroscopy; MD, molecular dynamics; NMR, nuclear magnetic resonance; NMV, *N*-methylvaline; NOE, nuclear Overhauser effect; NOESY, two-dimensional NOE spectroscopy; RMS, root mean squared; Sar, sarcosine (*N*-methylglycine); TOCSY, total correlated spectroscopy; TPPI, time-proportional phase incrementation.

0006-2960/94/0433-651$04.50/0

exocyclic guanine amino proton and the ActD threonine carbonyl oxygen, a weaker hydrogen bond between the guanine N3 and the ActD threonine amide proton, and stacking forces between the phenoxazone ring of the drug and the aromatic rings of the DNA bases (Sobell & Jain, 1972; Sobell, 1985). Additional stabilization of the complex results from hydrophobic interactions between minor groove surface atoms and the cyclic pentapeptides.

Several NMR investigations of complexes of ActD with oligonucleotides containing a single d(GC) binding site (Patel, 1974; Patel et al., 1981; Reid et al., 1983; Petersheim et al., 1984; Gorenstein et al., 1984; Brown et al., 1984; Jones et al., 1988; Delepierre et al., 1989; Liu et al., 1991), multiple binding sites (Scott et al., 1988a,b), and oligonucleotides containing no d(GC) binding sites (Zhou et al., 1989) have been reported. Intermolecular NOEs and changes in phosphorus and imino proton chemical shifts have been used to determine the binding site and to obtain information about the structural features of these complexes. The most important data are the intermolecular NOEs, which provide spatial interproton distance information. The three papers in which two-dimensional (2D) NOESY spectra were used (Brown et al., 1984; Delepierre et al., 1988; Liu et al., 1991) report a number of intermolecular NOEs, some of which are in disagreement with each other. NOEs from exchangeable protons were discussed in only one of these papers (Liu et al., 1991). In all of these studies, the oligonucleotides used were short, fully self-complementary fragments which form regular duplexes in the unbound state.

Because of the 2-fold symmetry of these self-complementary DNAs used in previous NMR studies of ActD binding, it has not been possible to quantify and characterize the two complexes formed due to the orientation of the asymmetric drug chromophore relative to the DNA axis. In an effort to better understand the manner in which ActD binds to DNA and the basis for its sequence specificity, we investigated the binding of the drug to an asymmetric DNA oligomer. Since perturbations in DNA structure may also influence drug binding, we chose to incorporate a DNA hairpin loop. Hairpin loops are important secondary structural elements in nucleic acids which can serve as recognition sites for proteins. One of the best characterized families of DNA hairpins contains four thymine nucleotides in the loop region. Previous structural investigations of these hairpins using X-ray crystallography, NMR spectroscopy, and thermodynamic measurements demonstrate the conformational heterogeneity possible in these structures—the reported crystal structure of d(CGCGCGTTTTCGCGCG) (Chattopadhyaya et al., 1988) differs significantly from its solution structure (Ikuta et al., 1986), particularly in the loop region. A detailed conformational analysis of the oligonucleotide d(CGCGTTTTCGCG) in solution using NOESY data and distance geometry calculations was carried out by Hare and Reid (1986). Because this sequence contains a single d(GC) step in the stem region, we chose to use this hairpin molecule for our investigation. The central four base pairs in the stem also correspond to the tetranucleotide used in a previous ActD–DNA NMR study (Delepierre et al., 1989). We included an AT base pair at the end of the stem, resulting in the sequence d(TCGCGTTTTCGCGA), to observe any effects from the drug's pentapeptide rings over a span of three nucleotides. The single adenine on the 3′ end also provides a convenient starting point for making sequential assignments of the DNA nucleotides.

Reported in this work are the complete assignments of the proton chemical shifts of the free DNA hairpin and the complexes formed by the binding of ActD to the oligonucleotide. The ^{31}P chemical shifts of the free DNA and of the complexes were also determined to confirm the intercalation site by monitoring the downfield shifts of the two phosphorous nuclei in the phosphodiesters which link G3 with C4 and G11 with C12. Also presented are models of the complexes based on interproton distance information which were extracted from NOESY experiments and used as constraints in molecular dynamics calculations. Two distinct ActD–d(TCGCGTTTTCGCGA) complexes are formed, which differ by the orientation with which the asymmetric chromophore intercalates the d(GC) step. The formation of multiple ActD–duplex DNA complexes has been reported (Jones et al., 1988; Scott et al., 1988a,b; Zhou et al., 1989), and we demonstrate that the mode of binding of ActD to this particular DNA hairpin is essentially the same as that which has been reported for standard double-stranded DNA (Brown et al., 1984). A total of 86 intermolecular contacts have been identified from NOESY spectra, including 27 involving exchangeable protons for each complex. The large number of intermolecular contacts provides the means for unambiguous elucidation of the chromophore orientation as well as both the DNA and drug conformations at the binding site of both complexes. This work represents what we believe to be the most detailed NMR investigation of multiple ActD–DNA complexes so far and the first example of the use of an asymmetric DNA oligomer in a NMR study of DNA-intercalating drugs.

MATERIALS AND METHODS

The oligonucleotide d(TCGCGTTTTCGCGA) was purchased from Pharmacia LKB Biotechnology, and actinomycin D was purchased from Sigma Chemical Co. Both compounds were used without further purification. Twenty-five milligrams of the DNA oligomers was dissolved in 1 mL of D_2O (Cambridge Isotope Labs, 99.96% enriched), and NaCl was added to a final salt concentration of 10 mM. The solution was divided into two equal portions, one of which was used to study the free DNA, while the other was used for the preparation of the ActD–DNA complex. The pH of each sample was measured in the NMR tube with a microelectrode and adjusted to pH 7.0, including correction for the isotope effect (Glasoe & Long, 1960). The ActD–DNA complex was formed by titrating the oligonucleotide solution with a stock solution of ActD in D_2O and monitoring the proton NMR spectrum until the resonances corresponding to the free DNA disappeared. The resulting solution of the ActD–DNA complex was dried down and redissolved in 0.40 mL of D_2O. For experiments in H_2O, the D_2O solvent was evaporated under a stream of nitrogen, and the sample was dissolved in a 90%/10% H_2O/D_2O solvent mixture.

Homonuclear NMR Spectroscopy. NMR spectra were collected on a Bruker AMX 500 spectrometer operating at 11.74 T. Phase-sensitive NOESY, double-quantum filtered COSY (DQF-COSY), and TOCSY spectra were acquired in absorption mode utilizing time-proportional phase incrementation (TPPI) (Marion & Wüthrich, 1983). Phase cycling permitted quadrature detection in t_1, and the spectrometer carrier offset was placed at the water solvent resonance frequency. NOESY spectra of the samples in D_2O were recorded with mixing times of 50, 100, 150, 200, 300, 400, and 500 ms for the free DNA hairpin and with mixing times of 50, 100, 150, and 500 ms for the complex. A continuous RF irradiation was applied during the recycle delay and during the mixing time of the NOESY experiments, to saturate the residual HOD resonance. For the experiments in H_2O,

NOESY mixing times of 250 ms were used for both samples and were performed with a 1–1 read pulse (Takahashi & Nagayama, 1989) to suppress the solvent peak. The pH was lowered to 5.9 in the H_2O samples to reduce the rate of imino proton exchange with the solvent. The temperatures which provided optimal dispersion of the proton resonances were 288 K for the free DNA hairpin sample and 298 K for the ActD–DNA complexes.

All of the homonuclear experiments in D_2O were acquired with a spectral width of 10 ppm, and spectral widths of 20 ppm were used for the proton experiments in H_2O. In all of the experiments, spectra were recorded with 512 increments in t_1 and 4096 complex points in t_2. For the NOESY spectra, 32 transients were averaged for each t_1 value, while 64 and 16 transients were averaged for the DQF-COSY and TOCSY spectra (70-ms mixing time), respectively. The data were apodized in both dimensions with Gaussian filters. Zero filling of the data produced 2D matrix sizes of 1K × 4K real points. The data were processed with the FELIX software package (Hare Research, Inc.) running on Silicon Graphics IRIS workstations.

Heteronuclear NMR Spectroscopy. The proton-detected ^{13}C heteronuclear multiple-quantum coherence (HMQC) spectrum of the ActD–DNA complex (data not shown) was obtained using the pulse sequence of Bax et al. (1986). A total of 64 transients were averaged for each of 512 increments in t_1, and 2048 complex points in t_2 were recorded. Spectral widths of 10 ppm in the proton dimension and 100 ppm in the carbon dimension were used. The $1/(2J_{HX})$ delays in the pulse sequence were optimized for proton–carbon coupling constants of approximately 150 Hz.

The ^1H–^{31}P scalar correlated 2D spectra were also obtained using the HMQC pulse sequence. A total of 64 transients were averaged for each of 200 t_1 increments, and 2048 complex points in t_2 were recorded. A spectral width of 4.5 ppm in the ^{31}P dimension and only 4 ppm in the proton dimension yielded very high resolution spectra. The $1/(2J_{HX})$ delays were optimized for proton–phosphorus coupling constants of approximately 7 Hz.

Structure Calculations. Molecular dynamics and energy minimization calculations were run on a Silicon Graphics Indigo workstation using the program X-PLOR (Brünger, 1992). For these calculations, distance constraints were extracted from the series of NOESY spectra (50, 100, 150, and 500 ms mixing times). The partial overlap of many of the cross-peaks in the NOESY spectrum of the two complexes precluded the integration of cross-peak intensities to determine interproton distances, so we carried out a qualitative categorization of NOE distance constraints. NOE cross-peaks with strong or very strong intensities (as determined from contour plots of the appropriate regions of the NOESY spectra) in the 50-ms mixing time NOESY spectrum were classified into distance constraints of 2.5–2.9 and 2.2–2.5 Å, respectively. NOE cross-peaks with medium intensity in the 50-ms spectrum which show strong intensity in the 100-ms mixing time spectrum were classified into distance constraints of 2.9–3.3 Å. Weak cross-peaks in the 50-ms spectrum which show medium intensity in the 100-ms spectrum were classified into distance constraints of 3.3–3.7 Å. Corresponding criteria for NOE cross-peaks in the 150- and 500-ms mixing time spectra yielded distance intervals of 3.7–4.1 and 4.1–6.0 Å. The different line shapes of protons with fewer homonuclear couplings (DNA base protons and methyl groups) compared to sugar and peptidic protons (which have slightly larger line widths due to their multiplet structures) were also taken into account when classifying cross-peak intensities. Observing the pattern of NOE intensity buildup for individual cross-peaks over the series of NOESY spectra allowed for a qualitative assessment of spin diffusion contributions to intensities. In those cases for which two cross-peaks are completely degenerate (one cross-peak arising from each complex), we assumed that the corresponding interproton distances were equal in both complexes with equal contributions to the combined cross-peak intensity. Pseudoatoms were used for individual methyl groups and nonstereospecifically resolved methylene protons and the interproton distances used for the structure calculations were adjusted accordingly (Wüthrich et al., 1983).

The geometries of the individual DNA sugars can be determined using a combination of both the scalar-coupled and the dipolar-coupled NMR data [for reviews, see, for example, Hosur et al. (1988), Van de Ven and Hilbers (1988), and Chou et al. (1992)]. Since all five possible torsion angles in the sugar ring are interdependent, the overall sugar conformation can be described as a function of the pseudorotation angle, P, and the pseudorotation amplitude, Φ_m. As a result, the DNA sugar pucker can be related to five three-bond coupling constants (^3J) or by nine interproton distances (not including individual interactions with the H5′ and H5″ sugar protons). The information from the ^3J and NOE values are complementary and allow for a detailed analysis of the sugar pucker. However, it is often the case that spectral overlap and line widths greater than the coupling constant being measured preclude a precise quantitation of cross-peak fine structure. Spectral overlap and strong spin diffusion effects also limit the utility of using NOEs to accurately determine interproton distances within the sugar ring. By plotting the dependence of these ^3J coupling constants and the interproton distances as a function of the pseudorotation angle, it can be seen that even though some coupling constants and interproton distances are somewhat insensitive to sugar pucker, all DNA sugar geometries (such as $C_{4'}$-*exo*, $O_{4'}$-*endo*, $C_{1'}$-*exo*, etc.) can be defined by a unique combination of interproton coupling constants and distances. Therefore, even in cases of spectral overlap, it is not difficult to obtain sugar puckering information by comparing magnitudes of coupling constants from the phase-sensitive DQF-COSY spectrum and relative NOESY cross-peak intensities. By using this method, sugar conformations were determined for all DNA bases in the free hairpin and in both complexes. These sugar conformations were then used to generate five idealized torsion angle restraints for each sugar in the subsequent calculations.

A total of 210 NOEs and 70 torsion angles (five per sugar moiety) were used as experimental constraints to determine the structure of the free DNA hairpin. A total of 86 intermolecular NOEs, 185 intra-DNA NOEs, 69 intra-ActD NOEs, and 70 torsion angles were used to determine each of the two ActD–DNA complexes. Since intrasugar NOEs were used to determine the individual sugar puckers as described above, these NOEs were not explicitly included as distance constraints in the calculations.

The starting structures for the calculations were generated within Insight (Biosym Technologies, Inc.), and the structure determinations were accomplished using a simulated annealing protocol. The slow cooling portion of the calculation involved 6 ps of molecular dynamics (0.002-ps time steps) to cool the system from 1500 K to a final temperature of 300 K in 50-deg steps (0.250 ps dynamics per temperature). A square-well potential function was used for the NOE restraints, and the scaling factor for the NOE energy term was increased at each temperature (from 5 to 30 kcal mol^{-1} $Å^{-2}$) during the molecular dynamics calculations. A square-well potential was also used

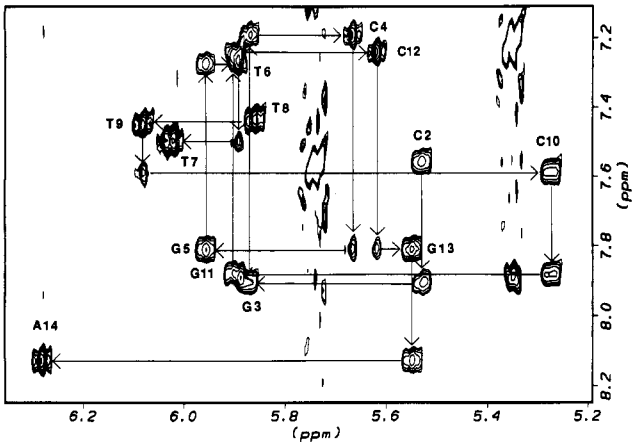

FIGURE 2: Expanded 500-MHz ^{1}H NOESY spectrum (mixing time, 500 ms) of 7 mM d(TCGCGTTTTCGCGA) in D_2O (base proton (H6/H8) to H1′ region), 15 °C, pH 7.0, 10 mM NaCl.

to constrain the sugar pucker torsion angles with a unity force constant (kcal mol^{-1} rad^{-2}) and a scaling factor of 30. The weighting factor for the non-symmetry-related van der Waal energy term was also gradually increased to prevent further changes in the global conformation as the system temperature was lowered. The final part of the calculation involved all-atom Powell conjugate gradient energy minimization. Hydrogen bond constraints were used throughout the calculations to maintain DNA base pairing and the double-helical nature of the hairpin stem.

A total of 20 structures were calculated for the free hairpin and for each of the two ActD–DNA complexes. All calculations were used to determine the respective average structures. Each average structure was then subjected to energy minimization to relieve improper bonds lengths and angles that arise as a result of the averaging protocol. This minimized average structure was then allowed to undergo 60 ps of dynamics with NOE and dihedral constraints enforced to yield the final structures. During the final 60-ps molecular dynamics calculation, the total energies of the structures were evaluated at each picosecond to confirm that a local energy minimum had been reached.

RESULTS

Resonance Assignments of the Free DNA Hairpin. Figure 2 shows the base proton (H6/H8) to deoxyribose H1′ region of a 500-ms NOESY spectrum, illustrating sequential assignments for the oligonucleotide. The pattern and relative intensities of the cross-peaks between the base and H1′ protons for nucleotides 1–5 and nucleotides 10–14 of the free hairpin indicate that the stem region forms a regular right-handed helical structure. Although a complete sequential assignment using the standard strategy for B-form DNA is not possible for this oligomer due to the absence of normal sequential NOEs between T7 and T8, internucleotide NOEs in other regions of the spectrum do permit a complete assignment. The sequence-specific resonance assignments are confirmed by ^{1}H–^{31}P HMQC experiments, which reveal correlations due to scalar couplings which occur between a backbone phosphorus nucleus and the H3′ proton on the 3′ side of the phosphodiester bond and the H4′, H5′, and H5″ protons on the 5′ side.

The 1D spectra of the exchangeable and nonexchangeable protons on d(TCGCGTTTTCGCGA) are shown in Figures 3–5. The resonance frequencies are very similar to those reported for other DNA hairpin structures with d(T)$_4$ loops (Haasnoot et al., 1983; Ikuta et al., 1986; Hare & Reid, 1986;

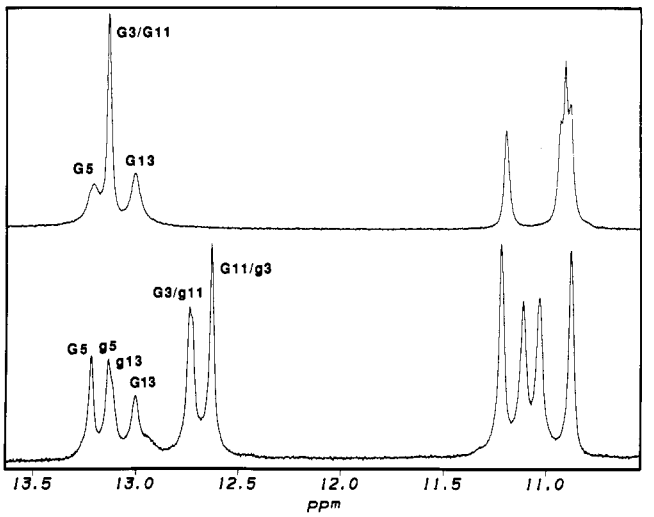

FIGURE 3: Imino regions of 500-MHz ^{1}H spectra of (a) d(TCGCGTTTTCGCGA) in H_2O, 15 °C, pH 5.9, 10 mM NaCl, and (b) ActD–d(TCGCGTTTTCGCGA) (1:1) in H_2O, 5 °C, pH 6.0, 10 mM NaCl. Note the upfield shifts of the imino protons of G3 and G11 in both complexes, as a result of intercalation by the drug. As expected for hairpin structures with d(T)$_4$ loops, the thymine imino proton resonances occur between 10.8 and 11.3 ppm. For Figures 3–6, uppercase letters refer to nucleotides in the major complex (complex A), while lowercase letters correspond to nucleotides in the minor complex (complex B).

Blommers et al., 1987). The exchangeable protons (Figure 3) gave rise to four signals in the range of 13.0–13.2 ppm, which were assigned to the imino protons of the two d(GC) and the two d(CG) base pairs, confirming the base-paired structure of the stem region. The thymine imino of the AT base pair was not observed, probably due to the increased exchange rate of imino protons in terminal basepairs. Four additional exchangeable resonances were attributed to the thymine imino protons from the nucleotides in the loop. At pH 7.0 (288 K), the rapid exchange rates of these non-base-paired imino protons caused extreme resonance broadening and could not be observed in the NMR spectrum. When the pH was lowered to 5.9, however, the resonances became narrow and observable, although the resonance due to the thymine imino proton of the AT base pair was still not observed. The chemical shift range of 10.9–11.2 ppm for these four resonances represents a significant upfield shift relative to the intrinsic chemical shift values for base-paired thymine imino protons which occur at around 14 ppm (Wüthrich, 1986). The upfield shift of these thymine imino protons is, however, characteristic of DNA hairpin structures with loop regions composed of four thymine nucleotides (Haasnoot et al., 1983).

Numerous NOEs involving the central four thymines were useful in characterizing the structure of the loop region. The identity of T6 was determined by NOEs from the methyl and H6 protons of T6 to the H1′, H2′, and H2″ protons of G5. Furthermore, a specific relative spatial orientation is evidenced by NOEs between T6Me and G5H8 protons, as well as between the T6H6 and G5H3′ protons. We determined the identity of T9 by NOEs from the H6 proton of C10 to the H1′, H2′, H2″, and H3′ protons of T9 and from the H5 proton of C10 to the H6, H2′, H2″, and methyl protons of T9.

Having identified several contacts between the nucleotides in the terminal base pair in the stem region (G5–C10) and nucleotides T6 and T9, the following NOEs are used to correlate the inner thymines of the loop (T7 and T8) with one another and with respect to T6 and T9. T7 was assigned by observing NOEs between the H1′ proton of T6 and the H6, Me, and H3′ protons of T7. The T6H2′ and T6H2″ protons both cross-relax the T7Me protons, while the T6H2′ proton

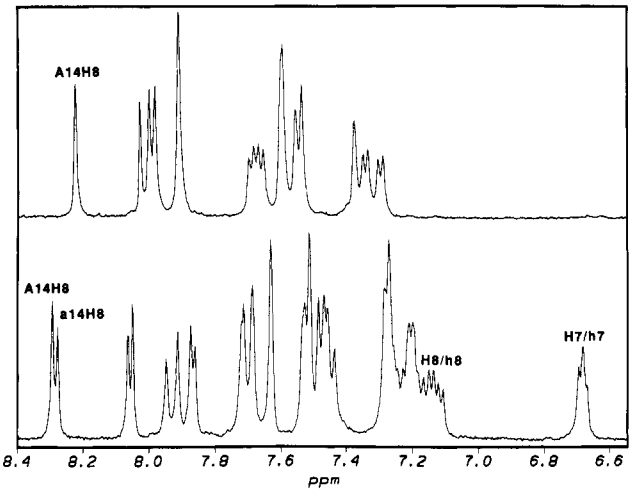

FIGURE 4: Aromatic regions of 500-MHz ^1H spectra of (a) d(TCGCGTTTTCGCGA) in D_2O, 15 °C, pH 7.0, 10 mM NaCl, and (b) ActD-d(TCGCGTTTTCGCGA) (1:1) in D_2O, 25 °C, pH 7.0, 10 mM NaCl. Note the doubling of the resonances in the complex, relative to the free DNA, which illustrates the formation of two distinct complexes. Also present in this region of the spectrum from the complex are resonances from the two aromatic protons on the drug chromophore (H7/h7 and H8/h8).

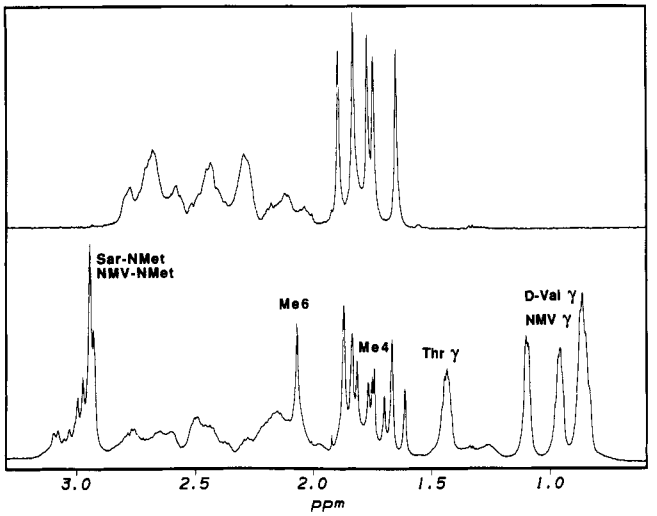

FIGURE 5: Aliphatic regions of 500-MHz ^1H spectra of (a) d(TCGCGTTTTCGCGA) in D_2O, 15 °C, pH 7.0, 10 mM NaCl, and (b) ActD–d(TCGCGTTTTCGCGA) (1:1) in D_2O, 25 °C, pH 7.0, 10 mM NaCl. Note the doubling of the thymine methyl resonances (1.6–1.9 ppm) and the appearance of additional signals resulting from drug protons.

is also in close proximity to the H4′ proton of T7. Connections between T8 and T7 are manifested by NOEs observed between the H1′, H3′, and H4′ protons on T7 and the methyl protons of T8. Also the T8H6 proton is cross-relaxed by the H2″ and H3′ protons of T7. Contacts between T8 and T9 include NOEs observed between the H1′, H2′, and H2″ protons of T8 and the T9Me protons, and between the H6 proton of T9 and the T8H1′ proton. The T8 methyl protons are also in close proximity to the H6, H1′, H2′, H2″, and H3′ protons of T6. The NOEs between the loop thymines and the presence of the thymine iminos seem to indicate that these nucleotides form some sort of a hydrophobic cluster.

Resonance Assignments of the Complex. The complexes were formed by titrating the stock solution of ActD into the free DNA solution. ActD binds very tightly to double-stranded DNA; the binding constant is on the order of 10^7 M^{-1} (Chen, 1988), and the two complexes are in slow exchange. After all of the free DNA had been titrated, two distinct sets of

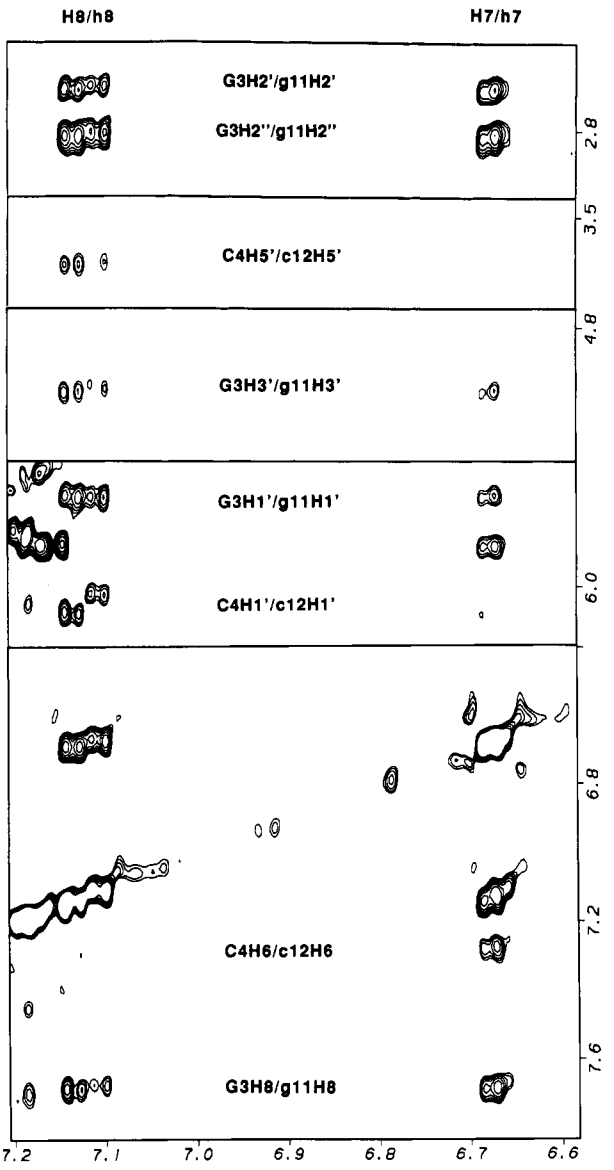

FIGURE 6: Regions of the 500-MHz NOESY spectrum of ActD–d(TCGCGTTTTCGCGA) (1:1) in D_2O, 25 °C, pH 7.0, 10 mM NaCl, which display intermolecular contacts between the phenoxazone chromophore protons (H7/h7 and H8/h8) and protons on the nucleotides at the intercalation site of the DNA hairpin. Since the aromatic chromophore protons are attached to the benzenoid side, for complex A only contacts to G3 and C4 are observed, whereas for complex B a very similar pattern is found for g11 and c12.

NMR resonances are present in an approximate ratio of 0.7:1.0. The formation of unequal amounts of the two complexes is readily apparent upon examination of the 1D spectrum found in Figures 4 and 5. The ratio of the intensities of the two resonances (one for each complex formed) for both the A14H8 and A14H2 protons is representative of the relative amounts of the two complexes present. These two sets of resonances result from the formation of two complexes which differ by the orientation with which the asymmetric drug chromophore intercalates the GC step. In complex A, the major complex, the benzenoid side of the chromophore is located on the side of the GC step formed by G3 and C4. Complex B is formed by a 180° rotation of the drug relative to the DNA helical axis, resulting in a structure with the benzenoid side of the phenoxazone ring stacked between G11 and C12. Due to the nearly symmetric nature of complex A relative to complex B, the chemical shifts of corresponding protons in the two complexes are quite similar. A standard sequential assignment of the DNA is not possible via the

Table I: Proton Chemical Shift Assignments of the DNA[a]

nucleotide	*b*	H8/H6	H5/H2/Me	H1′	H2′/H2″ [c]	H3′	H4′	H5′/H5″ [c]	amino	imino
T1	free	7.59	1.77	6.14	2.17/2.56	4.76	4.17	3.75		*e*
	complex A	7.48	1.61	6.08	2.06/2.43	4.63	4.12	3.73/3.67		*e*
	complex B	7.50	1.67	6.08	2.06/2.45	4.66	4.12	3.73/3.67		*e*
C2	free	7.66	5.84	5.63	2.26/2.49	4.90	4.19	4.08	8.76/7.18	
	complex A	7.16	5.89	5.66	1.25/1.85	4.61	3.94	*d*	8.69/7.22	
	complex B	7.26	5.85	5.73	1.48/1.88	4.74	3.96	*d*	8.62/7.32	
G3	free	8.00		5.98	2.77/2.72	5.04	4.43	4.14/4.08	*e*	13.13
	complex A	7.68		5.75	2.70/2.83	5.00	4.01	3.90	7.96/7.38	12.74
	complex B	7.72		5.76	2.63/2.78	4.96	4.02	3.87	8.32/7.46	12.63
C4	free	7.29	5.45	5.77	1.80/2.30	4.85	4.17	4.06	8.53/6.68	
	complex A	7.28	5.89	6.08	1.27/1.78	4.44	4.20	3.77	7.92/7.03	
	complex B	7.23	5.78	6.05	1.69/2.13	4.55	4.01	4.12/3.84	8.04/7.05	
G5	free	7.91		6.06	2.65	4.99	4.41	4.32/4.11	*e*	13.21
	complex A	7.91		6.00	2.76/2.64	5.01	4.45	4.04/3.94	*e*	13.22
	complex B	7.95		6.03	2.74/2.67	5.03	4.37	4.30/4.12	*e*	13.14
T6	free	7.37	1.74	5.99	2.10/2.43	4.84	4.20	4.12/3.99		(11.21/10.95/10.93/10.90)[f]
	complex A	7.48	1.85	6.08	2.17/2.42	4.85	4.28	4.12		(11.19/11.08/11.00/10.85)[g]
	complex B	7.55	1.85	6.14	2.24/2.45	4.87	4.27	4.11		(11.19/11.08/11.00/10.85)[g]
T7	free	7.60	1.83	6.12	2.12/2.40	4.65	4.21	4.15/4.00		(11.21/10.95/10.93/10.90)[f]
	complex A	7.63	1.88	6.13	2.15/2.39	4.68	4.26	4.10/4.01		(11.19/11.08/11.00/10.85)[g]
	complex B	7.63	1.88	6.13	2.15/2.39	4.68	4.26	4.10/4.01		(11.19/11.08/11.00/10.85)[g]
T8	free	7.53	1.65	5.96	2.03/2.27	4.72	4.05	3.95/3.76		(11.21/10.95/10.93/10.90)[f]
	complex A	7.51	1.67	5.94	2.06/2.30	4.73	4.04	3.94/3.81		(11.19/11.08/11.00/10.85)[g]
	complex B	7.53	1.72	5.97	2.10/2.32	4.73	4.08	3.95/3.86		(11.19/11.08/11.00/10.85)[g]
T9	free	7.55	1.89	6.18	2.36/2.59	4.73	4.27	4.04/3.86		(11.21/10.95/10.93/10.90)[f]
	complex A	7.45	1.81	6.06	2.26/2.48	4.72	4.19	3.96/3.89		(11.19/11.08/11.00/10.85)[g]
	complex B	7.44	1.76	6.06	2.20/2.44	4.72	4.18	3.96/3.90		(11.19/11.08/11.00/10.85)[g]
C10	free	7.69	5.85	5.37	2.31/2.43	4.85	4.20	4.07	8.65/7.24	
	complex A	7.20	5.84	5.74	1.33/1.81	4.70	3.93	*d*	8.72/7.36	
	complex B	7.19	5.88	5.67	1.44/1.88	4.65	3.99	*d*	8.84/7.32	
G11	free	7.98		6.00	2.67/2.77	5.04	4.42	4.14/4.08	*e*	13.13
	complex A	7.71		5.76	2.63/2.78	4.96	4.02	3.85	8.28/7.54	12.63
	complex B	7.69		5.75	2.70/2.83	5.00	4.01	3.90	7.85/7.53	12.71
C12	free	7.34	5.46	5.72	1.82/2.26	4.85	4.15	4.06	8.53/6.64	
	complex A	7.27	5.76	5.98	1.78/2.16	4.55	4.01	4.12/3.81	8.08/7.00	
	complex B	7.28	5.89	6.03	1.25/1.79	4.44	4.20	3.76	7.97/7.04	
G13	free	7.91		5.65	2.70	5.00	4.34	4.24/4.13	*e*	13.00
	complex A	7.87		5.60	2.60	4.96	4.26	4.09/3.96	*e*	13.00
	complex B	7.86		5.38	2.67/2.55	4.94	4.32	4.02/3.92	*e*	13.11
A14	free	8.22	8.04	6.38	2.67/2.45	4.73	4.28	4.21/4.14	*e*	
	complex A	8.30	8.05	6.39	2.78/2.51	4.75	4.26	4.14	*e*	
	complex B	8.28	8.07	6.41	2.72/2.51	4.72	4.29	4.16/4.19	*e*	

[a] Shifts referenced to sodium 3-trimethylsilyl propionate-*2,2,3,3-d*$_4$. [b] Complex A corresponds to the complex formed with the benzenoid side of ActD between G3 and C4 and between G11 and C12 for complex B. [c] The H2′ and H2″ protons are stereospecifically assigned. The H5′ and H5″ protons are not stereospecifically assigned. [d] Could not be unambiguously assigned due to overlap. The H5′ and H5″ protons are not stereospecifically assigned. [e] Could not be assigned due to exchange broadening. [f] The four imino resonances could not be unambiguously assigned due to a lack of relevant interproton NOEs. [g] The four imino resonances (corresponding to eight protons) could not be unambiguously assigned due to a lack of relevant interproton NOEs.

NOESY spectrum, as the DNA unwinds slightly upon intercalation of the chromophore. At the GC step where intercalation occurs, an effect of the unwinding of the DNA is that the distances between the sugar protons of G3 and the H6 proton of C4 and between the sugar protons of G11 and the H6 proton of C12 become too large to observe internucleotide NOEs, even after a long mixing time (500 ms). Nevertheless we can use the observed NOEs between the DNA nucleotides and the drug chromophore to confirm the DNA assignments at the intercalation site. The aromatic protons H7 and H8 of ActD are in close spatial proximity to G3 and C4 in complex A and to G11 and C12 in complex B (Figure 6). Therefore an indirect sequential assignment is possible, using the drug chromophore as an intermediate residue. A standard sequential assignment can be carried out from nucleotides T1 to G3 and C12 to A14 in both complexes, as all expected NOEs are observed between the base protons and the H1′, H2′, H2″, and H3′ on the 5′ neighboring nucleotides. The connections from G11 to C10 and from G3 to C2 are established with NOEs between the guanine base protons and the H2′, H2″, and H3′ protons on the cytosines. The chemical shifts of the H1′ protons on G3 and G11 in both complexes and the chemical shifts of C2H1′ in complex B and C10H1′ in complex A are nearly identical. These degeneracies prohibit the sequential assignment between these nucleotides in this region of the NOESY spectrum. For the case of C2H1′ in complex A and C10H1′ in complex B, although the chemical shifts differ from G3H1′ and G11H1′, respectively, no sequential NOEs are observed. The H6 proton of C10 experiences NOEs to the H2′ and H2″ protons of one thymine nucleotide, which is therefore assigned as T9. The H1′ protons of C10 and T9 also have very similar chemical shifts, and thus this sequential NOE is not discernible. Two thymine H6 protons cross-relax the H2′ and H2″ protons on the two remaining guanine deoxyribose rings, which therefore are assigned as G5 in the two different complexes. We also observe NOEs from these same thymine base protons to the H1′ and the H3′ protons of G5. These two thymines are therefore

assigned as T6 in the two complexes. The connection from G5 to C4 in complex A is established with NOEs which occur between the G5H8 proton and H1′, H2′, H2″, and H3′ protons of C4. In complex B the H1′ protons of C4 and G5 have nearly identical chemical shifts. C2H6 shows very weak NOEs to the H2′ and H2″ of one of the thymines, which therefore is assigned as T1, although no NOE is observed to the thymine H1′ proton. The assignment of T7 is made by observing a NOE from the T7H6 proton to the H3′ proton of T6 in the two complexes. It turns out that T7 is the only nucleotide which has nearly the same chemical shifts for all protons in both complexes (Table I). The chemical shifts of the H1′ protons on T6 and T7 are very similar; therefore, this sequential NOE is not detected. The only two nucleotides remaining to be assigned are the T8 nucleotides in both complexes. We can identify one sequential NOE between T9H6 and T8H4′, but no NOEs to the H1′, H2′, or H2″ protons of T8 are detectable. The resonances of the H3′ protons on T9 and T8 have essentially the same chemical shifts. In both complexes, there are no NOEs between the T8H6 protons and the sugar protons of T7, except for weak contacts to the H2″ protons.

The sequential assignment based on the homonuclear NOESY spectrum is also confirmed by a ^{1}H–^{31}P HMQC spectrum, as was done for the free DNA hairpin. Although, due to spectral overlap, not all phosphorus resonances in the two complexes are distinguishable, an unambiguous sequential assignment of the loop region was still possible.

Resonance Assignment of the Drug. Analogous to the situation regarding the proton resonance assignments for the DNA in the complexes, two sets of resonances are also observed for ActD in the complexes. For the drug, however, the problem of spectral overlap is even more pronounced—for each complex formed, there are two nearly identical sets of chemical shifts for the two pentapeptide rings connected to the benzenoid and quinoid sides of the chromophore (see Table II). Fortunately, differences between the chemical shifts of the chromophore H8 protons in the two complexes make it possible to distinguish between the complexes (see Figure 6). In the major complex (H8 at 7.14 ppm) we see several contacts to G3 and G4, whereas in the minor complex (H8 at 7.11 ppm) the same pattern of NOEs is obtained for G11 and C12. The NOEs between H7 and H8 on the chromophore and the methyl group of threonine allow the distinction between the benzenoid (Thr methyl at 1.42 ppm) and the quinoid (Thr methyl at 1.44 ppm) threonine, as only the threonine methyl groups on the benzenoid side of the chromophore should experience these NOEs. Therefore, the two different types of Thr H_α protons can be assigned in each of the two complexes (quinoid, 4.72/4.72; benzenoid, 4.96/4.95). For the Thr H_β protons, resonances are observed at 5.20 and 5.17 ppm, respectively. Both show contacts to a benzenoid Thr H_α proton and to a quinoid Thr H_α proton as well. There are no further contacts between the threonine methyl groups and other protons of the peptide chain which would allow unambiguous assignment of the resonances as either benzenoid or quinoid. Nevertheless, we observe NOEs from C4H1′ and C12H1′ to Pro H_β protons in both complexes. As discussed below, C4H1′ in complex A is near a H_β proton of the proline in the quinoid chain, while C12H1′ is proximate to a H_β proton on the benzenoid side. For complex B the situation is reversed. Thus it is possible to distinguish among four different Pro H_β protons, each of which belongs to a different complex and to a different peptide chain. By observing NOEs between proline H_α and H_β protons, it is clear that the benzenoid proline H_α protons appear at higher field (6.27 ppm) than the quinoid proline H_α protons (6.34 ppm), which is in agreement with previous investigations

Table II: Proton Chemical Shift Assignments of Actinomycin D[a]

residue	b	H^α	H^β	H^γ	H^δ	N-CH_3/NH
Thr	free (b)	4.82	5.24	1.29		c
	free (q)	4.66	5.27	1.30		c
	complex A (b)	4.97	5.21	1.43		8.00
	complex A (q)	4.73	5.18	1.45		8.14
	complex B (b)	4.96	5.18	1.43		8.06
	complex B (q)	4.73	5.21	1.45		8.09
D-Val	free (b)	3.55	2.08	1.00/0.76		8.11
	free (q)	3.59	2.10	1.00/0.77		8.01
	complex A (b)	3.60	2.17	1.10/0.88		8.25
	complex A (q)	3.64	2.19	1.10/0.87		8.25
	complex B (b)	3.59	2.17	1.10/0.88		8.25
	complex B (q)	3.64	2.19	1.10/0.87		8.25
Pro	free (b)	6.11	2.48/1.94	2.04	3.85/3.65	
	free (q)	6.22	2.45/1.94	2.04	3.77/3.67	
	complex A (b)	6.28	3.06/1.90	2.22	3.99/3.70	
	complex A (q)	6.35	3.10/1.97	2.12	4.03/3.74	
	complex B (b)	6.28	3.06/1.99	2.24	3.99/3.70	
	complex B (q)	6.35	3.10/1.97	2.12	4.03/3.74	
Sar	free (b)	4.68/4.18				2.80
	free (q)	4.74/4.17				2.79
	complex A (b)	4.67/4.26				2.93
	complex A (q)	4.65/4.31				2.95
	complex B (b)	4.72/4.30				2.95
	complex B (q)	4.69/4.31				2.93
Me-Val	free (b)	3.27	2.43	0.90/0.73		2.96
	free (q)	3.25	2.40	0.88/0.72		2.93
	complex A (b)	3.02	2.50	0.96/0.83		2.94
	complex A (q)	3.08	2.50	0.97/0.85		2.98
	complex B (b)	3.08	2.50	0.96/0.83		2.94
	complex B (q)	3.04	2.55	0.97/0.85		3.00

aromatics	$^{4}CH_3$	$^{6}CH_3$	H_7	H_8
free	1.73	2.43	7.38	7.38
complex A	1.75	2.07	6.69	7.15
complex B	1.75	2.07	6.68	7.12

[a] Shifts referenced to sodium 3-trimethylsilyl propionate-*2,2,3,3-d*$_4$. The data for the free drug were recorded at 288 K. [b] Complex A corresponds to the complex formed with the benzenoid side of ActD between G3 and C4 and between G11 and C12 for complex B. (b) = benzenoid side of chromophore; (q) = quinoid side of chromophore. [c] Could not be assigned because of exchange broadening.

(Delepierre et al., 1989). The very intense NOE between Pro H_α and D-Val H_α and the very weak NOEs between Pro H_β protons and D-Val H_α allow the assignment of the four D-Val spin systems. Contacts between D-Val H_α protons and the Sar H_α protons permit the assignment of the corresponding sarcosine resonances. The proline H_α protons also show NOEs to the *N*-methyl groups of Sar and *N*-methylvaline (NMV). To distinguish between the different *N*-methyl groups, we used the ^{13}C chemical shifts which we obtained from a HMQC experiment. The Sar *N*-methyl group carbon resonances appear at about 35 ppm, while the NMV *N*-methyl group carbon resonances occur at about 40 ppm. From the ^{13}C–H correlated experiments, we were then able to assign the chemical shifts of all *N*-methyl groups. With this knowledge we assigned the remainder of the protons in the NMV spin systems. The observation of a very weak NOE between the two Thr H_β resonances and the *N*-methyl groups of NMV allows the positive assignment of the different threonine spin systems, which was not possible previously (see above).

Intermolecular NOEs in D_2O. A total of 59 intermolecular NOEs between ActD and the DNA hairpin have been identified in the NOESY spectrum in D_2O for each complex. They are listed in Table III. Due to the frequency overlap of nearly all of the proton resonances from G3 in complex A with the corresponding resonances from G11 in complex B (and likewise for G11 in complex A and G3 in complex B), we can distinguish and specifically assign only those inter-

Table III: Intermolecular NOEs in the Actinomycin-D/Hairpin Complexes[a]

complex A	complex B	NOE	MD-(A)	MD-(B)	complex A	complex B	NOE	MD-(A)	MD-(B)
H7/C4H6	H7/C12H6	3.7–4.1	3.3	3.3	NMV-Met(b)/G3H3′	NMV-Met(b)/G11H3′	4.1–7.0	6.5	6.5
H7/C4H5	H7/C12H5	3.3–3.7	3.9	3.6	NMV-Met(q)/G11H3′	NMV-Met(q)/G3H3′	4.1–7.0	6.6	6.4
H7/G3H8	H7/G11H8	3.7–4.1	3.4	3.5	NMV-Met(b)/G3H5′	NMV-Met(b)/G11H5′	4.1–7.0	5.0	4.9
H7/G3H1′	H7/G11H1′	4.1–6.0	4.5	4.2	NMV-Met(q)/G11H5′	NMV-Met(q)/G3H5′	4.1–7.0	4.9	4.8
H7/G3H2′	H7/G11H2′	3.7–4.1	4.0	4.0	NMV-Met(b)/C2H1′	NMV-Met(b)/C10H1′	3.3–4.7	4.4	4.2
H7/G3H2″	H7/G11H2″	2.9–3.3	3.4	3.0	NMV γ^d(b)/G3H1′	NMV γ^d(b)/G11H1′	4.1–7.0	5.7	6.0
H7/G3H3′	H7/G11H3′	4.1–6.0	5.8	5.6	NMV γ^d(q)/G11H1′	NMV γ^d(q)/G3H1′	4.1–7.0	6.0	6.1
H8/G3H8	H8/G11H8	4.1–6.0	4.1	4.5	NMV γ^d(b)/G3H4′	NMV γ^d(b)/G11H4′	2.2–3.5	2.7	3.1
H8/G3H1′	H8/G11H1′	3.3–3.7	3.1	3.0	NMV γ^d(q)/G11H4′	NMV γ^d(q)/G3H4′	2.2–3.5	2.8	3.1
H8/G3H2′	H8/G11H2′	3.3–3.7	3.6	3.9	NMV γ^d(b)/G3H5′	NMV γ^d(b)/G11H5′	3.3–4.7	4.0	4.0
H8/G3H2″	H8/G11H2″	2.2–2.5	2.1	2.2	NMV γ^d(q)/G11H5′	NMV γ^d(q)/G3H5′	3.3–4.7	3.9	3.9
H8/C4H1′	H8/C12H1′	4.1–6.0	3.8	4.2	NMV γ^h(b)/G3H4′	NMV γ^h(b)/G11H4′	4.1–7.0	4.5	4.8
H8/C4H5′	H8/C12H5′	3.7–4.1	4.4	3.6	NMV γ^h(q)/G11H4′	NMV γ^h(q)/G3H4′	4.1–7.0	4.7	5.0
Met6/C4H5	Met6/C12H5	3.3–4.7	4.1	4.1	NMV γ^h(b)/G3H5′	NMV γ^h(b)/G11H5′	4.1–7.0	4.8	4.8
Met6/G3H8	Met6/G11H8	3.7–5.1	4.5	4.6	NMV γ^h(q)/G11H5′	NMV γ^h(q)/G3H5′	4.1–7.0	4.6	4.8
Met6/C4H6	Met6/C12H6	3.7–5.1	4.9	5.2	exchangeable protons				
Met4/C12H5	Met4/C4H5	3.7–5.1	4.7	4.7	Met4/G3H1	Met4/G11H1	2.9–4.3	4.6	4.4
Met4/G11H8	Met4/G3H8	3.7–5.1	4.5	4.5	Met4/G11H1	Met4/G3H1	4.1–7.0	5.4	5.6
Thr γ(b)/G3H2′	Thr γ(b)/G11H2′	3.7–5.1	5.0	5.1	Met4/C12H4(1)	Met4/C4H4(1)	3.3–4.7	3.3	3.2
Thr γ(q)/G11H2′	Thr γ(q)/G3H2′	3.7–5.1	5.0	5.0	Met4/C12H4(2)	Met4/C4H4(2)	3.3–4.7	3.3	3.2
Thr γ(b)/G3H2″	Thr γ(b)/G11H2″	3.3–4.7	3.6	3.9	Met6/G11H1	Met6/G3H1	2.9–4.3	4.3	4.6
Thr γ(q)/G11H2″	Thr γ(q)/G3H2″	3.3–4.7	3.9	3.7	Met6/C4H4(1)	Met6/C12H4(1)	3.3–4.7	3.5	3.2
Thr γ(b)/G3H1′	Thr γ(b)/G11H1′	2.2–3.5	3.3	3.3	Met6/C4H4(2)	Met6/C12H4(2)	3.3–4.7	3.3	3.3
Thr γ(q)/G11H1′	Thr γ(q)/G3H1′	2.2–3.5	3.2	3.0	Thr-NH(b)/G3H2(1)	Thr-NH(b)/G11H2(1)	3.3–3.7	4.0	4.0
Thr γ(b)/G3H8	Thr γ(b)/G11H8	4.1–7.0	6.2	6.4	Thr-NH(q)/G11H2(1)	Thr-NH(q)/G3H2(1)	3.3–3.7	3.8	3.9
Thr γ(q)/G11H8	Thr γ(q)/G3H8	4.1–7.0	6.3	6.1	Thr-NH(b)/G3H1′	Thr-NH(b)/G11H1′	2.9–3.3	2.8	2.9
Thr γ(b)/C4H1′	Thr γ(b)/C12H1′	4.1–7.0	6.4	6.4	Thr-NH(q)/G11H1′	Thr-NH(q)/G3H1′	2.9–3.3	2.9	2.9
Thr γ(b)/C4H3′	Thr γ(b)/C12H3′	4.1–7.0	6.7	6.5	Pro α(b)/G3H1	Pro α(b)/G11H1	4.1–6.0	5.9	5.9
Thr γ(b)/C4H5′	Thr γ(b)/C12H1′	3.7–5.1	4.7	4.8	Pro α(q)/G11H1	Pro α(q)/G3H1	4.1–6.0	5.8	5.5
Thr γ(q)/C12H5′	Thr γ(q)/C4H5′	3.7–5.1	4.9	4.2	Pro β^d(q)/G5H1	Pro β^d(q)/G5H1	4.1–6.0	5.8	5.9
Pro β^d(b)/C12H1′	Pro β^d(b)/C4H1′	3.7–4.1	3.8	3.6	Pro β^d(q)/G11H1	Pro β^d(q)/G3H1	3.7–4.1	4.2	4.7
Pro β^d(q)/C4H1′	Pro β^d(q)/C12H1′	3.7–4.1	3.6	3.5	Sar α^d(b)/G3H1	Sar α^d(b)/G11H1	4.1–6.0	5.8	5.8
NMV α(b)/G3H1′	NMV α(b)/G11H1′	3.7–4.1	3.4	3.7	Sar α^d(q)/G11H1	Sar α^d(q)/G3H1	4.1–6.0	5.1	4.6
NMV α(q)/G11H1′	NMV α(q)/G3H1′	3.7–4.1	3.7	3.7	Sar α^h(b)/G3H1	Sar α^h(b)/G11H1	4.1–6.0	6.7	6.8
NMV α(b)/G3H4′	NMV α(b)/G11H4′	2.2–2.5	2.1	2.2	Sar α^h(q)/G11H1	Sar α^h(q)/G3H1	4.1–6.0	6.2	5.7
NMV α(q)/G11H4′	NMV α(q)/G3H4′	2.2–2.5	2.2	2.3	Sar α^d(q)/G5H1	Sar α^d(b)/G5H1	4.1–6.0	5.4	5.2
NMV α(b)/G3H3′	NMV α(b)/G11H3′	4.1–6.0	4.7	4.9	Sar α^h(q)/G5H1	Sar α^h(b)/G5H1	4.1–6.0	5.6	4.9
NMV α(q)/G11H3′	NMV α(q)/G3H3′	4.1–6.0	4.7	4.9	NMVMet(b)/G3H1	NMVMet(b)/G11H1	2.9–4.3	4.9	4.8
NMV α(b)/G3H5′	NMV α(b)/G11H5′	3.7–4.1	3.9	3.7	NMVMet(q)/G11H1	NMVMet(q)/G3H1	2.9–4.3	4.6	4.8
NMV α(q)/G11H5′	NMV α(q)/G3H5′	3.7–4.1	3.5	3.6	NMVMet(b)/G3H2(1)	NMVMet(b)/G11H2(1)	3.3–4.7	4.0	4.1
NMV-Met(b)/G3H1′	NMV-Met(b)/G11H1′	3.3–4.7	3.9	3.7	NMVMet(q)/G11H2(1)	NMVMet(q)/G3H2(1)	3.3–4.7	4.0	4.2
NMV-Met(q)/G11H1′	NMV-Met(q)/G3H1′	3.3–4.7	4.0	3.9	NMVMet(q)/G5H1	NMVMet(b)/G5H1	2.9–4.3	4.6	4.8
NMV-Met(b)/G3H4′	NMV-Met(b)/G11H4′	3.3–4.7	4.5	4.5	NMVMet(b)/G13H1	NMVMet(q)/G13H1	4.1–7.0	6.3	6.7
NMV-Met(q)/G11H4′	NMV-Met(q)/G3H4′	3.3–4.7	4.6	4.4					

[a] In the case of resolved but nonstereospecifically assigned methylene protons, d = downfield resonance and h = highfield resonance.

molecular NOEs for which the chemical shifts of the corresponding drug protons differ in the two complexes. This is the case for all of the contacts between the DNA and the aromatic protons of the chromophore (H7 and H8). Similar intermolecular NOE patterns between these drug protons and DNA protons are observed for both complexes. Thus it can be concluded that the conformation at the binding site of complex B is nearly identical to that of complex A.

In complex A several NOEs were observed between the aromatic protons of the chromophore and nucleotides G3 and C4. In support of these observations, the methyl group on the quinoid ring ($^4CH_3$) experiences weak NOEs to G11H8 and C12H5 (see Table III). Nearly all contacts between the peptide chains and the DNA are also concentrated in the G3/C4 or G11/C12 regions. G3 and C4 experience most of their intermolecular NOEs to the protons on the Thr and NMV residues in the benzenoid peptide chain, and the same pattern of NOEs are present between G11 and C12 and the Thr and NMV residues in the quinoid peptide chain. As mentioned above, the situation is reversed for the H_β protons of proline, where the quinoid proline H_β proton is close to the H1′ proton of C4 and the benzenoid proline H_β proton is close to the H1′ proton of C12. The only contacts of other nucleotides to the drug take place between C2H1′ and the *N*-methyl group of NMV in the benzenoid peptide chain. It is also the only intermolecular NOE which has no corresponding NOE on the quinoid side of the complex (see Table III). In contrast to others (Delepierre et al., 1989), we do not detect any NOEs between Sar or D-Val protons and the DNA.

For complex B, a pattern of NOEs is revealed which is analogous to those observed for complex A. All of the contacts observed in complex A between the drug and G3/C4 now occur between the drug and G11/C12. This is also true for the other side of the binding site (G11/C12 in A becomes G3/C4 in B). Therefore the drug intercalates in two different orientations, maintaining its overall conformation.

Intermolecular NOEs Involving Exchangeable Protons. The NOESY spectrum in H_2O permits not only the assignment of imino and amino protons of the nucleotides but also the assignment of the peptide amide protons of Thr and D-Val. Contrary to what would be expected for normal B-DNA, for the ActD–DNA hairpin complex, cross-peaks are observed between the imino protons of G3 and G11 and their corresponding guanine amino protons. Even though they may be involved in hydrogen bonds, the exocyclic guanine amino protons are usually exchange broadened by rotation about the C–N bond, and no such cross-peaks are observed (Rajagopal et al., 1988). This indeed is the situation observed for the free DNA hairpin. However, in the ActD–DNA complexes, the rotation of these amino protons, which are located in the minor

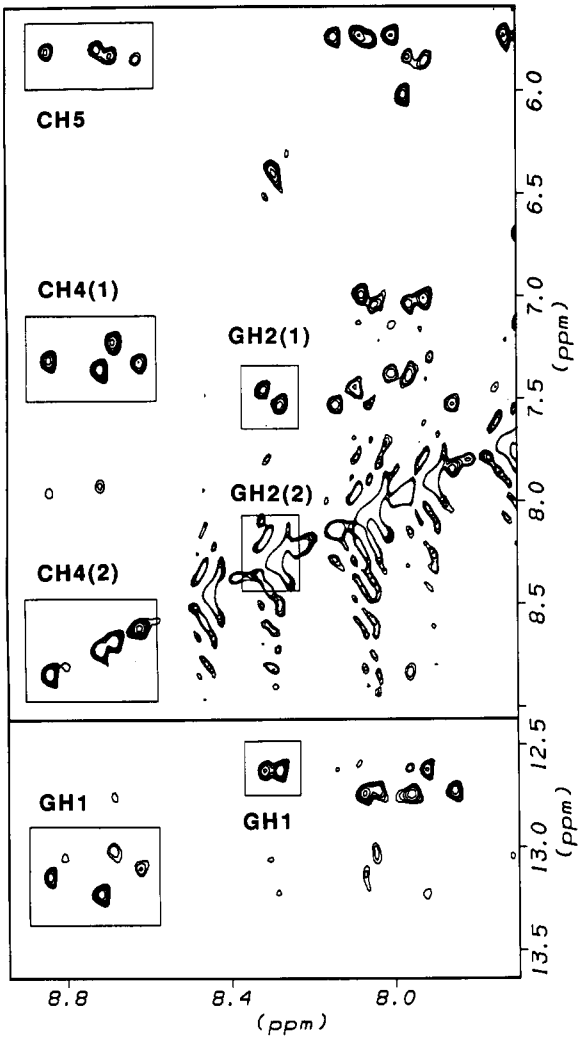

FIGURE 7: Amino/imino and the amino/amino regions of the 500-MHz NOESY spectrum of ActD–d(TCGCGTTTTCGCGA) (1:1) in H_2O, 5 °C, pH 6.0, 10 mM NaCl, which show the unusual presence of the G3 and G11 imino/amino cross-peaks (smaller GH1 box in the lower panel, see text). NOEs between the G5 and G13 imino protons and the amino protons of the base-paired cytosines (C10 and C2, respectively) are outlined in the larger GH1 box in the lower panel. Cytosine amino protons, labeled CH4(1) and CH4(2), can be distinguished from those of the guanine due to the additional NOEs to the cytosine H5 protons (CH5).

groove of DNA, seems to be hindered. Figure 7 shows the imino/amino and the amino/amino region of the NOESY spectrum in H_2O. It is obvious that only G3 and G11 show the additional cross-peaks, whereas G5 and G13 show the normal pattern of two amino protons attached to the corresponding cytosine. The amino protons of cytosine and guanine are easily distinguished, as only the cytosine amino protons are cross-relaxed by an H5 proton. The semiquantitative analysis of the NOESY cross-peaks reveals several important NOEs which occur between drug protons and exchangeable protons on the DNA. Each of the two methyl groups on the drug chromophore experience NOEs to the imino and the amino protons of G3, C4, G11, and C12, which also supports the idea of the formation of two complexes by intercalation of the phenoxazone ring in the two orientations described above.

The NOEs involving the peptide amide protons help to further define the structure of the two peptide chains. We observe very intense cross-peaks between the threonine amide protons and the H1′ protons of C4 and C12. They appear due to their participation in intermolecular hydrogen bonds with the N3 atoms of G3 and G11. It should be mentioned that,

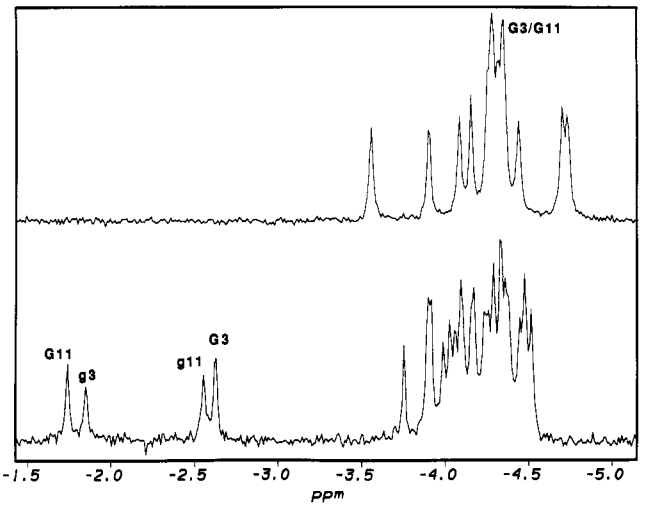

FIGURE 8: ^{31}P spectra at 202.4 MHz of (a) d(TCGCGTTTTCGCGA) in D_2O, 15 °C, pH 7.0, 10 mM NaCl, and (b) ActD–d(TCGCGTTTTCGCGA) (1:1) in D_2O, 25 °C, pH 7.0, 10 mM NaCl. The spectra are referenced to trimethylphosphate. Note the downfield shifts of the phosphorus nuclei in the phosphodiester groups which link the nucleotides at the site of intercalation (G3 and G11). It is also apparent from the intensities of the resonances that the two complexes are formed in unequal amounts.

due to fast exchange with the solvent, the threonine amide protons were not observed in the spectra of free ActD in H_2O. In complex A, the very weak NOEs between the imino proton of G11 and the Sar H_α protons in the quinoid peptide chain and between the imino proton of G3 and the Sar H_α protons in the benzenoid peptide chain are the only intermolecular contacts to these amino acids. All intermolecular NOEs involving exchangeable protons are also listed in Table III. As mentioned earlier, the pH was adjusted to about 6.0 to observe the four thymine iminos in the loop region. Although they appear as very sharp signals at 10.6–11 ppm, only the imino at the highest field shows a very weak NOE to the imino proton of G5 in complex A. There is also a NOE cross-peak between two thymine imino protons, but as there are no intrathymine correlations, we could not unambiguously assign the four thymine imino resonances.

^{31}P-NMR. Previous investigations (Patel et al., 1981) have shown that the chemical shifts of the phosphorus nuclei in the DNA backbone which link the nucleotides forming the GC step will shift toward lower field upon chromophore intercalation. Figure 8 shows the phosphorus 1D spectra of the free DNA and of the 1:1 mixture with ActD. It is obvious that four resonances experience a significant shift to lower field. A ^1H–^{31}P HMQC spectrum was recorded (Figure 9) to assign these signals, which were found to belong to the G3/C4 and the G11/C12 linking phosphodiester groups, respectively. As seen in Table IV, the phosphorus nuclei on the quinoid side appear at lower field (G11 in complex A; G3 in complex B) than the atoms on the benzenoid side (G3 in complex A; G11 in complex B). Another interesting result is that the phosphorus nuclei which belong to the residues in the loop region do not show any unusual chemical shifts. This is in contrast to previous publications which found a correlation between changes in the deoxyribose–phosphate backbone and the phosphorus chemical shifts (Gorenstein et al., 1984). As mentioned above, ^1H–^{31}P HMQC is a very powerful technique for sequential assignment, especially in those cases for which insufficient internucleotide NOEs are available.

DISCUSSION

Conformation of the Free Hairpin. All DNA glycosidic torsion angles are in the *anti* conformation, as determined

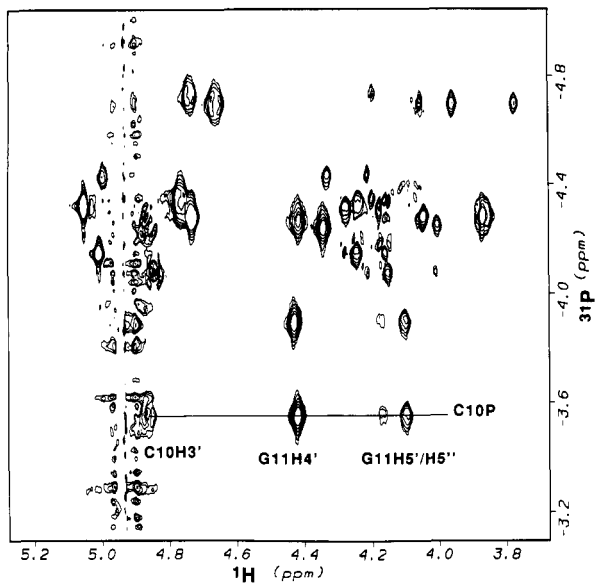

FIGURE 9: ^1H–^{31}P HMQC spectrum of d(TCGCGTTTTCGCGA) in D_2O, 15 °C, pH 7.0, 10 mM NaCl. A total of 1024 points in t_2, 128 scans per t_1 block, and 200 t_1 values were acquired. Each phosphorus resonance is correlated via scalar coupling to an H3′ proton in the 3′ direction and to the H4′, H5′, and H5″ protons in the 5′ direction.

Table IV: ^{31}P Chemical Shifts[a]

	free	complex A	complex B		free	complex A	complex B
T1	−4.30	−4.10	−4.15	T8	−4.27	−4.29	−4.34
C2	−3.90	*b*	*b*	T9	−4.75	*b*	*b*
G3	−4.32	−2.61	−1.84	C10	−3.55	−4.42	−4.39
C4	−4.25	−4.24	−4.11	G11	−4.32	−1.73	−2.55
G5	−4.45	−4.19	−4.31	C12	−4.23	−4.03	−4.23
T6	−4.09	−3.89	−3.99	G13	−4.16	−3.92	−3.75
T7	−4.71	−4.52	−4.49				

[a] Shifts referenced to trimethylphosphate. [b] Could not be unambiguously assigned due to overlap.

from the observation of weak NOEs between the base protons and the H1′ proton on the same nucleotide and the strong NOE between the base proton and the H2′ proton. The cross-peak intensities in the NOESY spectrum between the base and sugar protons indicate that the stem region of the hairpin adopts a standard B-form-like conformation. Due to appreciable overlap in the sugar proton region of the DQF-COSY, TOCSY, and NOESY spectra, a more qualitative approach to determining deoxyribose sugar puckers was adopted, as described earlier. It is important to note that quantitative analysis of antiphase cross-peaks, especially within the practical limits of digital resolution, often leads to inaccurate measurements of coupling constants when the resonance line widths are close to or greater than the coupling constant being measured (Neuhaus et al., 1985). A consequence of this phenomenon is that the magnitude of the coupling constant is proportional to the intensity of the cross-peak (Neuhaus et al., 1985; Hosur et al., 1988). Because of these considerations, we have tabulated coupling constants as a range of values (Table V) as opposed to a single value. Detailed analysis of molecular dynamics simulations have shown that pseudorotation angles are inherently subject to large fluctuations (Swaminathan et al., 1991). Although, if only one coupling constant is used to define the sugar pucker, these ranges may cause differences up to 50° in the pseudorotation angle, by analyzing the three coupling constants most sensitive to sugar pucker, ^3J(H1′,H2′), ^3J(H2″,H3′), and ^3J(H3′,H4′), we can reduce the number of possible sugar conformations consistent with the data and thus define the individual sugar puckers.

In the free DNA hairpin, two different sugar puckering modes were observed: C_1′-*exo* and C_2′-*endo*. In both cases a strong coupling constant is found for ^3J(H1′,H2′), ^3J(H1′,H2″), and ^3J(H2′,H3′), with ^3J(H1′,H2′) > ^3J(H1′,H2″) = ^3J(H2′,H3′), and an weak, almost undetectable coupling constant for ^3J(H2″,H3′). The experimentally measurable difference between the two sugar puckers is the magnitude of the J(H3′,H4′) coupling constant. In the case of the C_1′-*exo* orientation, the coupling constant is about 3 Hz, and in the case of the C_2′-*endo* conformation the coupling constant is close to 0 Hz and no cross-peak is observed (Hosur et al., 1988; Van de Ven & Hilbers, 1988). The C_1′-*exo* conformation is found for all cytosines, T6, T9, and A14, whereas all guanines, T7, and T8 have a C_2′-*endo* pucker. This analysis does not consider that the sugars may exist in multiple conformations. Unfortunately, due to overlap of the cross-peaks arising from the two symmetry-related complexes, we were not able to employ the methods described by Rinkel and Altona (1987) of analyzing the sums of the sugar proton couplings. Therefore, the possibility that the sugars may be exchanging between different sugar puckers (Schmitz et al., 1990) cannot be ruled out.

An interesting feature that has previously been reported as characteristic of $d(T)_4$ loop structures is the presence of a thymine–thymine "wobble" base pair, formed between the first and fourth thymines in the loop (Haasnoot et al., 1983; Hare & Reid, 1986; Blommers et al., 1987). Evidence for the existence of this unusual base pair has been founded on interpreting NOEs between these two thymine residues and the terminal base pair in the DNA stem as being indicative of base stacking. The cross-peak between two thymine imino protons has also been used as evidence for "wobble" base pairing between the first and last thymines in the loop. However, it is difficult to unambiguously assign the thymine imino protons in regions of nonregular DNA structure due to a lack of additional information from intraresidue correlations or any other internucleotide NOEs. The loop structure that we obtained from our restrained molecular dynamics and energy minimization calculations does not contain a thymine–thymine "wobble" base pair, but rather T6, T7, and T9 point toward each other to form a hydrophobic pocket. T8, on the other hand, appears to be oriented away from this cluster of nucleotides, possibly the result of steric hindrance or sugar–phosphate backbone conformational limitations. Additional calculations from different starting loop structures consistently provided the same result with well-satisfied NOE distance and dihedral constraints. In our calculated structure, the aforementioned imino–imino NOE can be attributed to the interaction between T6 and T7, and both of these imino protons are in close proximity to the imino proton of G5.

DNA Conformation in the Two Complexes. A comparison of the chemical shifts of the free DNA and the two complexes (Table I) shows that there are some significant changes in proton resonance frequencies upon ActD binding. Interestingly, the largest changes do not occur at the intercalation site (G3, C4, G11, C12) but rather for the flanking cytosines, C2 and C10. It is also worth noting that the chemical shifts of the loop region do not change very much. A comparison of the two different complexes shows a very similar set of chemical shifts with the exception of the H2′ and H2″ protons of C4 and C12 and the unusually highfield shift of the H1′ proton of G13 in complex B. The NOESY spectrum exhibits a similar pattern of inter-DNA cross-peaks as was found for the free hairpin. The increased spectral overlap caused by the presence

Table V: Coupling Constants and NOEs Used To Determine DNA Sugar Geometries[a]

residue	b	^3J(H1′,H2′) (Hz)	^3J(H2″,H3′) (Hz)	^3J(H3′,H4′) (Hz)	H1′/H4′ NOE (Å)	H2″/H4′ NOE (Å)
T1	free	6–9	0–3	0–3	2.9–3.3	3.3–3.7
	complex A	6–9	0–3	3–6	3.3–3.7	3.3–3.7
	complex B	6–9	0–3	0–3	3.3–3.7	3.3–3.7
C2	free	6–9	0–3	0–3	2.9–3.3	4.1–6.0
	complex A	0–3	0–3	6–9	2.9–3.3	3.3–3.7
	complex B	3–6	0–3	6–9	3.3–3.7	4.1–6.0
G3	free	3–6	0–3	0–3	2.9–3.3	3.3–3.7
	complex A	3–6	0–3	0–3	3.3–3.7	4.1–6.0
	complex B	3–6	0–3	0–3	3.3–3.7	4.1–6.0
C4	free	6–9	0–3	3–6	2.9–3.3	3.7–4.1
	complex A	0–3	0–3	0–3	4.1–6.0	3.3–3.7
	complex B	3–6	0–3	3–6	3.3–3.7	3.3–3.7
G5	free	3–6	0–3	0–3	2.9–3.3	3.3–3.7
	complex A	6–9	0–3	0–3	3.3–3.7	4.1–6.0
	complex B	6–9	0–3	0–3	3.3–3.7	3.7–4.1
T6	free	3–6	0–3	3–6	2.9–3.3	3.3–3.7
	complex A	3–6	0–3	6–9	3.3–3.7	3.3–3.7
	complex B	3–6	0–3	6–9	4.1–6.0	3.3–3.7
T7	free	6–9	0–3	0–3	3.3–3.7	4.1–6.0
	complex A	6–9	0–3	0–3	3.3–3.7	4.1–6.0
	complex B	6–9	0–3	0–3	3.3–3.7	4.1–6.0
T8	free	6–9	0–3	0–3	2.9–3.3	3.3–3.7
	complex A	6–9	0–3	0–3	3.3–3.7	3.3–3.7
	complex B	3–6	0–3	0–3	3.3–3.7	4.1–6.0
T9	free	6–9	0–3	3–6	2.9–3.3	3.7–4.1
	complex A	6–9	0–3	3–6	4.1–6.0	3.7–4.1
	complex B	6–9	0–3	3–6	4.1–6.0	3.7–4.1
C10	free	6–9	0–3	0–3	2.9–3.3	3.3–3.7
	complex A	3–6	0–3	6–9	3.3–3.7	3.3–3.7
	complex B	6–9	0–3	6–9	3.3–3.7	3.3–3.7
G11	free	0–3	0–3	0–3	3.3–3.7	3.3–3.7
	complex A	0–3	0–3	0–3	3.3–3.7	4.1–6.0
	complex B	0–3	0–3	0–3	3.3–3.7	4.1–6.0
C12	free	6–9	0–3	3–6	2.9–3.3	3.7–4.1
	complex A	6–9	0–3	3–6	3.7–4.1	3.3–3.7
	complex B	0–3	0–3	0–3	3.3–3.7	3.3–3.7
G13	free	6–9	0–3	0–3	2.9–3.3	4.1–6.0
	complex A	6–9	0–3	0–3	2.9–3.3	3.3–3.7
	complex B	6–9	0–3	0–3	2.9–3.3	3.7–4.1
A14	free	6–9	0–3	3–6	2.9–3.3	3.3–3.7
	complex A	6–9	0–3	3–6	3.3–3.7	3.3–3.7
	complex B	6–9	0–3	3–6	3.7–4.1	4.1–6.0

[a] Due to factors such as spectral overlap, coupling constants are presented as a range of values (see text). [b] Complex A corresponds to the complex formed with the benzenoid side of ActD between G3 and C4 and between G11 and C12 for complex B.

of two distinct complexes makes a quantitative analysis of coupling constants and NOE intensities even more problematic than described for the free hairpin above. However, the cross-peak patterns and intensities in the phase-sensitive DQF-COSY spectrum (Figure 10) are almost identical to the free DNA indicating that similar sugar puckers are present in the two complexes as were determined for the free hairpin. Therefore, even after intercalation by ActD, the stem region maintains a B-form-like conformation (with some concomitant unwinding at the intercalation site). The RMS difference between the energy-minimized average DNA structures in the two complexes is 1.10 Å.

The small changes in chemical shift as well as similar NOESY and DQF-COSY cross-peak patterns indicate that the conformation of the loop region does not change appreciably upon intercalation with the drug. The pairwise RMS deviation between the free DNA loop region and the loop region from the two complexes is 1.68 Å, and only 0.43 Å between the two complexes. Again, there is no concrete evidence for "wobble" base pairs in either complex.

Conformation of ActD. A comparison of the proton chemical shifts for the pentapeptide rings in the free and bound states shows that no significant changes occur upon binding (see Table II). The strong NOEs between Pro α and D-Val α, as well as the NOE between Pro α and Sar α, are the most obvious signs that there is no change in the overall conformation of the two peptide rings upon binding. These NOEs indicate that the D-Val-Pro peptide bonds and the Pro-Sar peptide bonds in both complexes adopt *cis* configurations, which is the same as observed for the free ActD in solution (data not shown). The side chain conformations of the peptide residues in the free drug and in a complex with d(CGCG) were previously determined (Delepierre et al., 1989) to favor a *trans* conformation for D-Val and NMV, whereas Thr showed preference for a *gauche* orientation. These results were deduced from $^3J(H_\alpha/H_\beta)$ coupling constants and NOE measurements. In the case presented here, the results from the NOESY spectrum are in agreement with these previous studies. For D-Val and NMV, only a weak NOE is observed between their respective α and β protons, which indicates a *trans* orientation. For Thr this NOE is much more intense, as would be expected for a *gauche* conformation.

Conformation of the ActD–DNA Complexes. Molecular Dynamics Simulation. Several molecular dynamics (MD)

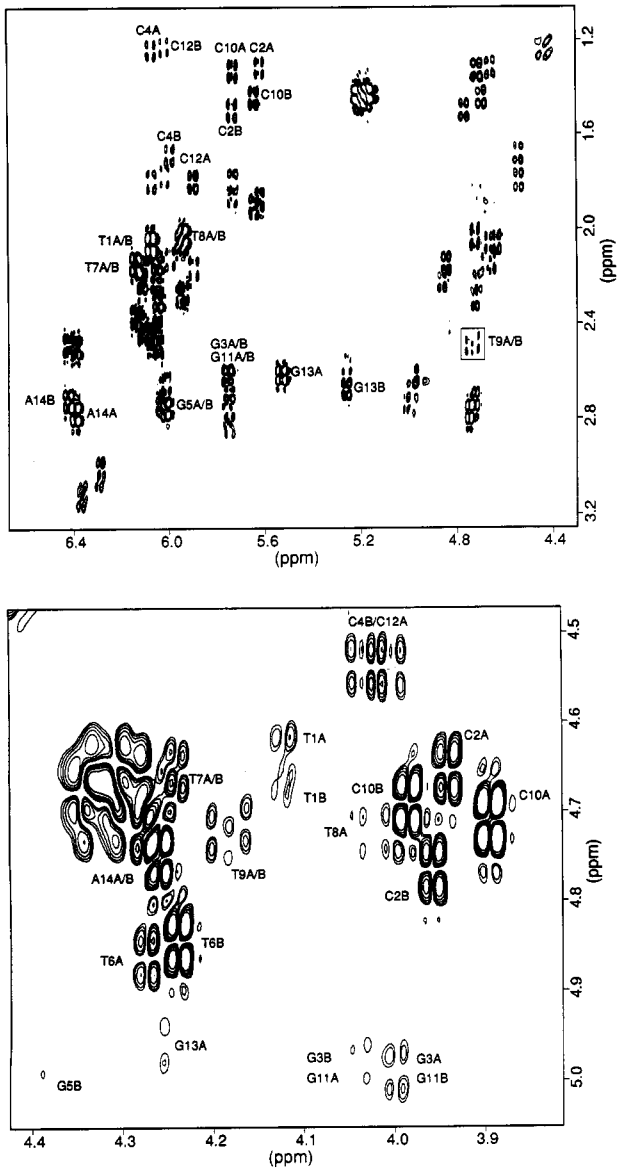

FIGURE 10: Expanded regions of the DQF-COSY spectrum of the ActD–DNA complexes used for defining the individual sugar puckers. Both positive and negative (stippled lines) peaks are plotted. (a, top) The H1′,H2′/H2″ and H2′/H2″,H3′ region. The H1′,H2′ cross-peaks are labeled with their assignment in either complex A, B, or both. The only H2″,H3′ cross-peak that is observed (boxed) arises from T9. (b, bottom) The H3′,H4′ cross-peak region.

simulations of ActD–DNA complexes have been published. In some cases no experimental data (i.e., NOEs and coupling constants) were used as constraints (Lybrand et al., 1986). In the paper of Delepierre et al. (1989), molecular mechanics calculations were carried out, "using some of the semi-quantitative distances given by NOE effects as constraints during minimization". No further details were given. A very detailed description is presented by Creighton et al. (1989). Among several free calculations they also present a restrained MD calculation using the NOEs of a previous NMR investigation (Brown et al., 1984). In the paper of Liu et al. (1991), NOE constraints, resulting from NOE buildup rates, were used in two MD simulations. However, the authors do not comment on how well the experimental data are fulfilled in the calculated structures.

Intermolecular NOEs. Reid et al. (1983) used 1D NOE techniques and assigned 14 NOEs between the tetranucleotide d(AGCT) and ActD, all of which are in agreement with our results. In a study of the complex of ActD with d(CGCG) (Delepierre et al., 1989), several NOEs were mentioned

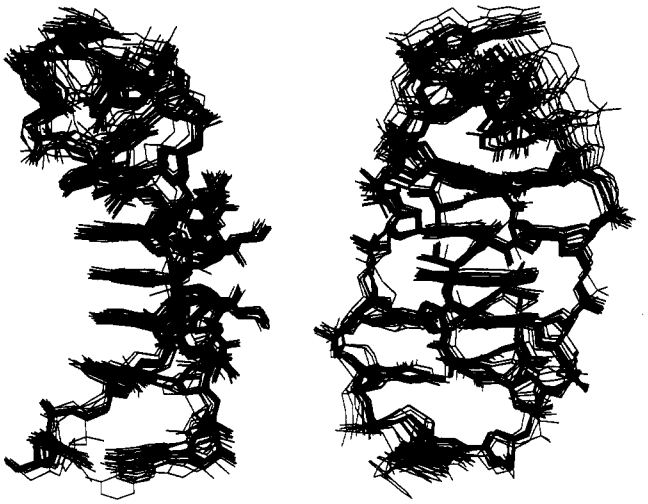

FIGURE 11: Two views of 20 superimposed structures for one of the ActD–DNA complexes by restrained molecular dynamics using experimentally derived distance constraints. Protons are not shown for clarity.

explicitly (less than 20); however, it is not clear if those represent the total number of NOEs that were observed. Some of the NOEs are contradictory to our findings. For example, they discussed NOEs from the Sar-NMet groups to the DNA, while no NOEs were found for the NMV-NMet groups. We document nine correlations between the NMV-NMet groups and protons on the nucleotides but no NOEs between the Sar-NMet groups and the DNA. They also assert that no NOEs between the methyl groups on the chromophore and the DNA are present, while we have identified 12 NOEs of this type. Additionally, we observe several contacts between the ActD H7 and H8 protons and the protons on G2 and C3 at the intercalation site. Brown et al. (1984) studied a complex of ActD with the oligonucleotide d(ATGCAT), for which they uncovered 27 drug–DNA NOEs. The most detailed investigation so far was carried out by Patel and co-workers (Liu et al., 1991), who report 70 intermolecular NOEs between ActD and d(AAAGCTTT), most of which are in reasonably good agreement with our results. From a study of ActD binding to d(ATGCGCAT) (Scott et al., 1988a,b), the formation of two different complexes was observed, which were distinguished by the different orientation of the chromophore. These results were supported on the basis of ^{31}P NMR and the chemical shifts of the imino protons without detailed NOE data.

In the present investigation, as expected, the chromophore intercalates exclusively at the lone d(GC) step, formed from nucleotides G3, C4, G11, and C12. This result was verified by the observation of NOEs between protons on the chromophore and protons on these nucleotides. No other nucleotides were involved in NOEs with the drug chromophore protons. NOEs observed between protons in the peptide residues of the drug and protons in the minor groove of the DNA hairpin provide evidence for the binding of the peptides to the minor groove. The resulting structure from 20 calculations for complex A is shown in Figure 11, and the energy-minimized average structures (also averaged over 60 ps of dynamics) for both complexes are shown in Figure 12.

The binding of ActD to DNA does not seem to be adversely affected by the presence of a hairpin loop two base pairs removed from the intercalation site. The total pairwise RMS difference over all atoms of the four drug peptides (two per complex) in the calculated structures is only 0.72 Å. This result suggests that if the hairpin loop is far enough removed

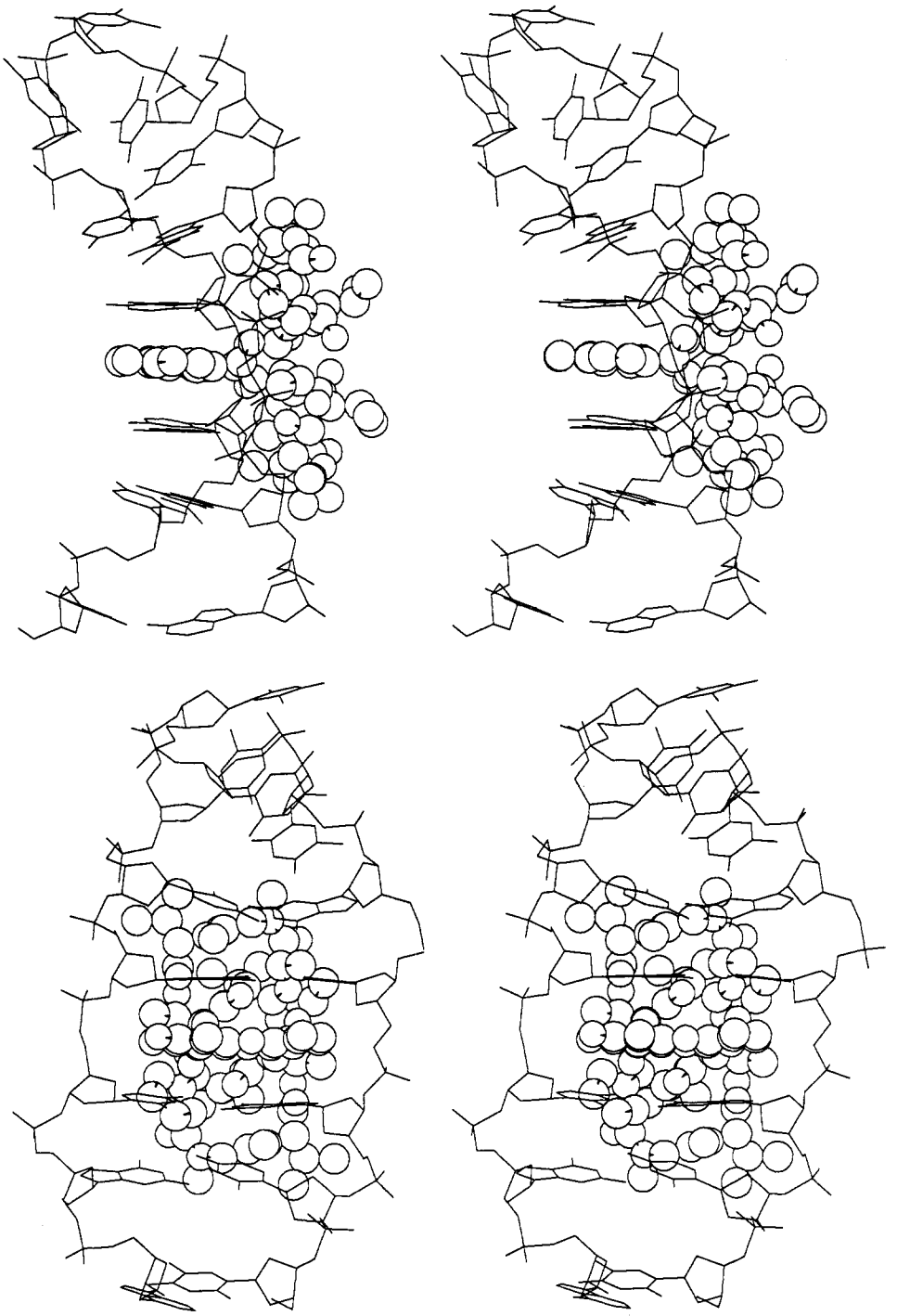

FIGURE 12: Two stereoviews of the energy minimized average structure of complex A. The ActD molecule is displayed as spheres (radius = 0.5 van der Waals radius), and protons are not shown for clarity. (A, top) Side view. (B, bottom) View looking into the major groove of the DNA oligomer.

from the intercalation site as to not effect the geometry of the DNA minor groove at the peptide binding site, then the peptide conformation is dictated by the DNA duplex and therefore may be recognizing specific DNA sequences. However, if the hairpin loop is perturbing the minor groove geometry at the peptide binding site, the symmetry of the four cyclic peptides in the calculated structures suggests that they are rigid structural elements compared to the DNA backbone. If this is the case, ActD may show preferential binding to d(GC) sites with adjacent base pair sequences that exhibit increased backbone flexibility or bending. We are currently pursuing these possibilities by using heteronuclear coupling constants (^{1}H–^{31}P and ^{13}C–^{31}P) to better define the DNA phosphate backbone for comparisons of hairpin backbone conformations in the free and ActD-bound states, and we are studying ActD complexes with hairpin DNAs with varying numbers of base pairs between the intercalation site and the $d(T)_4$ loop.

Although intermolecular NOEs are only observed between ActD and the four bases in the intercalation site and the two flanking base pairs, ActD binding affects the local environment of other base pairs as evidenced by the doubling of the adenine resonances. We are particularly interested in investigating why the two nearly identical complexes are not formed in equal concentrations. Two possibilities exist: either there is a sequence dependence for base pairs neighboring the d(GC) intercalation site or the proximity of the hairpin loop may induce steric constraints which exaggerate the electrostatic effects of the intercalation site. We are now studying

complexes of ActD bound to analogous DNA sequences in order to address this question.

ACKNOWLEDGMENT

This work was supported by grants from the American Cancer Society (CH-32M and DHP-240). D.R.B. was partially supported by the NIH (GM40635 to D.R.K.). We are grateful to the NIH (1S01 RR03342) and the NSF (BBS86-12359) for providing resources for the acquisition of the 500-MHz NMR instrument.

REFERENCES

Bax, A., & Subramanian, S. (1986) *J. Magn. Reson. 67*, 565–569.

Blommers, M. J. J., Haasnoot, C. A. G., Hilbers, C. W., van Boom, J. H., & van der Marel, G. A. (1987) in *Structure and Dynamics of Biopolymers, NATO ASI Ser. E 133*, 78–91.

Brown, S. C., Mullis, K., Levenson, C., & Shafer, R. H. (1984) *Biochemistry 23*, 403–408.

Brünger, A. T. (1992) *X-PLOR Version 3.0 Manual*, Yale University, New Haven, CT.

Chattopadhyaya, R., Ikuta, S., Grzeskowiak, K., & Dickerson, R. E. (1988) *Nature (London) 334*, 175–179.

Chen, F.-M. (1988) *Biochemistry 27*, 6393–6397.

Chou, S.-H., Cheng, J.-W., & Reid, B. R. (1992) *J. Mol. Biol. 228*, 138–155.

Creighton, S., Rudolph, B., Lybrand, T., Singh, U. C., Shafer, R., Brown, S., Kollman, P., Case, D. A., & Andrea, T. (1989) *J. Biomol. Struct. Dyn. 6*, 929–969.

Delepierre, M., van Heijenoort, C., Igolen, J., Pothier, J., Le Bret, M., & Roques, B. P. (1989) *J. Biomol. Struct. Dyn. 7*, 557–589.

Fox, K. R., & Waring, M. J. (1984) *Nucleic Acids Res. 12*, 9271–9285.

Glasoe, P. K., & Long, F. A. (1960) *J. Phys. Chem. 64*, 188–190.

Goldberg, I. H., & Rabinowitz, M. (1962) *Science 136*, 315–316.

Gorenstein, D. G., Lai, K., & Shah, D. O. (1984) *Biochemistry 23*, 6717–6723.

Haasnoot, C. A. G., de Bruin, S. H., Berendsen, R. G., Janssen, H. G. J. M., Binnendijk, T. J. J., Hilbers, C. W., van der Marel, G. A., & van Boom, J. H. (1983) *J. Biomol. Struct. Dyn. 1*, 115–129.

Hare, D. R., & Reid, B. R. (1986) *Biochemistry 25*, 5341–5350.

Hosur, R. V., Govil, G., & Miles, H. T. (1988) *Magn. Reson. Chem. 26*, 927–944.

Ikuta, S., Chattopadhyaya, R., Ito, H., Dickerson, R. E., & Kearns, D. R. (1986) *Biochemistry 25*, 4840–4849.

Jain, S. C., & Sobell, H. M. (1972) *J. Mol. Biol. 68*, 1–20.

Jones, R. L., Scott, E. V., Zon, G., Marzilli, L. G., & Wilson, W. D. (1988) *Biochemistry 27*, 6021–6026.

Kirk, J. M. (1960) *Biochim. Biophys. Acta 42*, 167–169.

Lane, M. J., Dabrowiak, J. C., & Vournakis, J. N. (1983) *Proc. Natl. Acad. Sci. U.S.A. 80*, 3260–3264.

Liu, X., Chen, H., & Patel, D. J. (1991) *J. Biomol. NMR 1*, 323–347.

Lybrand, T. P., Brown, S. C., Creighton, S., Shafer, R. H., & Kollman, P. A. (1986) *J. Mol. Biol. 191*, 495–507.

Mauger, A. B. (1980) in *Topics in Antibiotic Chemistry*, Vol. 5, 229–305, Ellis Horwood, Chichester, England.

Marion, D., & Wüthrich, K. (1983) *Biochem. Biophys. Res. Commun. 113*, 967–974.

Muller, W., & Crothers, D. M. (1968) *J. Mol. Biol. 35*, 251–290.

Neuhaus, D., Wagner, G., Vasak, M., Kägi, J. H. R., & Wüthrich, K. (1985) *Eur. J. Biochem. 151*, 257–272.

Patel, D. J. (1974) *Biochemistry 13*, 2396–2402.

Patel, D. J., Koglowski, S. A., Rice, J. A., Broka, C., & Itakura, K. (1981) *Proc. Natl. Acad. Sci. U.S.A. 78*, 7281–7284.

Petersheim, M., Mehdi, S., & Gerlt, J. A. (1984) *J. Am. Chem. Soc. 106*, 439–440.

Rajagopal, P., Gilbert, D. E., van der Marel, G. A., van Boom, J. H., & Feigon, J. (1988) *J. Magn. Reson. 78*, 526–537.

Reich, E., Franklin, R. M., Shatkin, A. J., & Tatum, E. L. (1961) *Science 134*, 556–557.

Reid, D. G., Salisbury, S. A., & Williams, D. H. (1983) *Biochemistry 22*, 1377–1385.

Rehfuss, R., Goodisman, J., & Dabrowiak, J. C. (1990) in *Molecular Basis of Specificity in Nucleic Acid–Drug Interactions* (Pullman, B., & Jortner, J., Eds.) pp 157–166, Kluwer Academic, Holland.

Rinkel, L. J., & Altona, C. (1987) *J. Biomol. Struct. Dyn. 4*, 621–649.

Schmitz, U., Zon, G., & James, T. L. (1990) *Biochemistry 29*, 2357–2368.

Scott, E. V., Jones, R. L., Banville, D. L., Zon, G., Marzilli, L. G., & Wilson, W. D. (1988a) *Biochemistry 27*, 915–923.

Scott, E. V., Zon, G., Marzilli, L. G., & Wilson, W. D. (1988b) *Biochemistry 27*, 7940–7951.

Sobell, H. M. (1985) *Proc. Natl. Acad. Sci. U.S.A. 82*, 5328–5331.

Sobell, H. M., & Jain, S. C. (1972) *J. Mol. Biol. 68*, 21–34.

Takahashi, S., & Nagayama, K. (1989) *J. Magn. Reson. 81*, 555–560.

Van de Ven, J. M., & Hilbers, C. W. (1988) *Eur. J. Biochem. 178*, 1–38.

Waring, M. J. (1970) *J. Mol. Biol. 54*, 247–279.

Wüthrich, K. (1986) in *NMR of Proteins and Nucleic Acids*, p 34, Wiley-Interscience, New York.

Wüthrich, K., Billeter, M., & Braun, W. (1983) *J. Mol. Biol. 169*, 949–961.

Zhou, N., James, T. L., & Shafer, R. H. (1989) *Biochemistry 28*, 5231–5239.